high $\Delta^{13}CH_3D$ values at CROMO suggest that methane here could be sourced from a mixture of thermogenic and microbial methane. Alternatively, lower H_2 availability at CROMO, compared with The Cedars (table S4), may support microbial methanogenesis under near-equilibrium conditions (Fig. 4). Regardless, the different isotopologue signatures in methane from CROMO versus The Cedars demonstrate that distinct processes contribute to methane formation in these two serpentinization systems.

Deep, ancient fracture fluids in the Kidd Creek mine in the Canadian Shield (*31*) contain copious quantities of both dissolved methane and hydrogen (*5*). The Kidd Creek methane occupies a distinct region in the diagram of $\Delta^{13}CH_3D$ versus $\varepsilon_{methane/water}$ (Fig. 2), due to strong D/H disequilibria between methane and water (*4*) and low–$\Delta^{13}CH_3D$ temperature signals of 56° to 90°C that are consistent with other temperature estimates for these groundwaters (*4*). Although the specific mechanisms by which the proposed abiotic hydrocarbons at Kidd Creek are generated remain under investigation (*5*, *32*), the distinct isotopologue signals provide further support for the hypothesis that methane here is neither microbial nor thermogenic.

Our results demonstrate that measurements of $^{13}CH_3D$ provide information beyond the simple formation temperature of methane. The combination of methane and water hydrogen-isotope fractionation and $^{13}CH_3D$ abundance enables the differentiation of methane that has been formed at extremely low rates in the subsurface (*3*, *21*, *27*) from methane formed in cattle and surface environments in which methanogenesis proceeds at comparatively high rates (*33*, *34*).

REFERENCES AND NOTES

1. F. J. Baldassare, M. A. McCaffrey, J. A. Harper, *Am. Assoc. Pet. Geol. Bull.* **98**, 341–372 (2014).
2. R. M. Flores, C. A. Rice, G. D. Stricker, A. Warden, M. S. Ellis, *Int. J. Coal Geol.* **76**, 52–75 (2008).
3. J. Pohlman, M. Kaneko, V. Heuer, R. Coffin, M. Whiticar, *Earth Planet. Sci. Lett.* **287**, 504–512 (2009).
4. B. Sherwood Lollar *et al.*, *Geochim. Cosmochim. Acta* **72**, 4778–4795 (2008).
5. B. Sherwood Lollar, T. D. Westgate, J. A. Ward, G. F. Slater, G. Lacrampe-Couloume, *Nature* **416**, 522–524 (2002).
6. J. Welhan, J. Lupton, *Am. Assoc. Pet. Geol. Bull.* **71**, 215–223 (1987).
7. M. J. Whiticar, *Org. Geochem.* **16**, 531–547 (1990).
8. R. A. Burke Jr., C. S. Martens, W. M. Sackett, *Nature* **332**, 829–831 (1988).
9. C. K. McCalley *et al.*, *Nature* **514**, 478–481 (2014).
10. M. J. Whiticar, E. Faber, M. Schoell, *Geochim. Cosmochim. Acta* **50**, 693–709 (1986).
11. G. Etiope, B. Sherwood Lollar, *Rev. Geophys.* **51**, 276–299 (2013).
12. M. Schoell, *Chem. Geol.* **71**, 1–10 (1988).
13. M. J. Whiticar, *Chem. Geol.* **161**, 291–314 (1999).
14. S. Ono *et al.*, *Anal. Chem.* **86**, 6487–6494 (2014).
15. D. A. Stolper *et al.*, *Geochim. Cosmochim. Acta* **126**, 169–191 (2014).
16. D. A. Stolper *et al.*, *Science* **344**, 1500–1503 (2014).
17. D. L. Valentine, A. Chidthaisong, A. Rice, W. S. Reeburgh, S. C. Tyler, *Geochim. Cosmochim. Acta* **68**, 1571–1590 (2004).
18. E. P. Reeves, J. S. Seewald, S. P. Sylva, *Geochim. Cosmochim. Acta* **77**, 582–599 (2012).
19. Materials and methods are available as supplementary materials on *Science* Online.
20. R. Burruss, C. Laughrey, *Org. Geochem.* **41**, 1285–1296 (2010).
21. B. L. Bates, J. C. McIntosh, K. A. Lohse, P. D. Brooks, *Chem. Geol.* **284**, 45–61 (2011).
22. E. P. Reeves, J. M. McDermott, J. S. Seewald, *Proc. Natl. Acad. Sci. U.S.A.* **111**, 5474–5479 (2014).
23. The abundance of $^{13}CH_3D$ is captured by a metric, $\Delta^{13}CH_3D$, that quantifies its deviation from a random distribution of isotopic substitutions among all isotopologues in a sample of methane: $\Delta^{13}CH_3D = \ln Q$, where Q is the reaction quotient of the isotope exchange reaction $^{13}CH_4 + {}^{12}CH_3D \rightleftharpoons {}^{13}CH_3D + {}^{12}CH_4$. The reported δ values are conventional isotopic notation, e.g., $\delta D = (D/H)_{sample}/(D/H)_{reference} - 1$. Mass spectrometric measurements yield Δ_{18}, a parameter that quantifies the combined abundance of $^{13}CH_3D$ and $^{12}CH_2D_2$. For most natural samples of methane, Δ_{18} temperature is expected to be directly relatable to $\Delta^{13}CH_3D$ temperature, as measured by laser spectroscopy. The D/H fractionation between methane and environmental water is defined as $\varepsilon_{methane/water} = (D/H)_{methane}/(D/H)_{water} - 1$.
24. M. Balabane, E. Galimov, M. Hermann, R. Letolle, *Org. Geochem.* **11**, 115–119 (1987).
25. C. Rees, *Geochim. Cosmochim. Acta* **37**, 1141–1162 (1973).
26. B. A. Wing, I. Halevy, *Proc. Natl. Acad. Sci. U.S.A.* **111**, 18116–18125 (2014).
27. T. Holler *et al.*, *Proc. Natl. Acad. Sci. U.S.A.* **108**, E1484–E1490 (2011).
28. R. A. Burke Jr., *Chemosphere* **26**, 55–67 (1993).
29. P. L. Morrill *et al.*, *Geochim. Cosmochim. Acta* **109**, 222–240 (2013).
30. D. Cardace *et al.*, *Sci. Drill.* **16**, 45–55 (2013).
31. G. Holland *et al.*, *Nature* **497**, 357–360 (2013).
32. B. Sherwood Lollar, T. C. Onstott, G. Lacrampe-Couloume, C. J. Ballentine, *Nature* **516**, 379–382 (2014).
33. K. A. Johnson, D. E. Johnson, *J. Anim. Sci.* **73**, 2483–2492 (1995).
34. C. Varadharajan, H. F. Hemond, *J. Geophys. Res.* **117**, G02004 (2012).
35. K. Takai *et al.*, *Proc. Natl. Acad. Sci. U.S.A.* **105**, 10949–10954 (2008).
36. Y. Horibe, H. Craig, *Geochim. Cosmochim. Acta* **59**, 5209–5217 (1995).

ACKNOWLEDGMENTS

We thank J. Hayes, R. Summons, A. Whitehill, S. Zaarur, C. Ruppel, L. T. Bryndzia, N. Blair, D. Vinson, K. Nealson, and M. Schrenk for discussions; W. Olszewski, D. Nelson, G. Lacrampe-Couloume, and B. Topçuoğlu for technical assistance; A. Whitehill, G. Luo, A. Appril, K. Twing, W. Brazelton, A. Wray, J. Oh, A. Rowe, G. Chadwick, and A. Rietze for assistance in the field; R. Michener for the δD_{water} analyses; L. T. Bryndzia (Shell) for providing the shale gas samples; R. Dias (USGS) for sharing the NGS samples; and R. Raiche, D. McCrory, S. Moore (Homestake Mining Co.), the staff of the McLaughlin Natural Reserve, and the well operators for access to samples. Grants from the NSF (EAR-1250394 to S.O. and EAR-1322805 to J.C.M.), N. R. Braunsdorf and D. J. H. Smit of Shell PTI/EG (to S.O.), the Deep Carbon Observatory (to S.O., B.S.L., M.K., and K.-U.H.), the Natural Sciences and Engineering Research Council of Canada (to B.S.L.), and the Gottfried Wilhelm Leibniz Program of the Deutsche Forschungsgemeinschaft (HI 616-14-1 to K.-U.H. and M.K.) supported this study. D.T.W. was supported by a National Defense Science and Engineering Graduate Fellowship. D.S.G. was supported by the Neil a nd Anna Rasmussen Foundation Fund, the Grayce B. Kerr Fellowship, and a Shell-MITEI Graduate Fellowship. Any use of trade, firm, or product names is for descriptive purposes only and does not imply endorsement by the U.S. government. All data used to support the conclusions in this manuscript are provided in the supplementary materials. Author contributions: D.T.W. and S.O. developed the methods, analyzed data, and performed modeling. D.T.W. and D.S.G. performed isotopic analyses. D.S.G., L.C.S., J.F.H., M.K., K.-U.H., and S.O. designed and/or conducted microbiological experiments. D.T.W., D.S.G., B.S.L., P.L.M., K.B.D., A.N.H., C.N.S., M.D.K., D.J.R., J.C.M., D.C., and S.O. designed and/or executed the field-sampling campaigns. D.T.W. and S.O. wrote the manuscript with input from all authors.

SUPPLEMENTARY MATERIALS

www.sciencemag.org/content/348/6233/428/suppl/DC1
Materials and Methods
Supplementary Text
Figs. S1 to S5
Tables S1 to S6
References (*37*–*87*)

5 December 2014; accepted 18 February 2015
Published online 5 March 2015;
10.1126/science.aaa4326

ISOTOPE GEOCHEMISTRY

Biological signatures in clumped isotopes of O_2

Laurence Y. Yeung,[1,2]*† Jeanine L. Ash,[1]*† Edward D. Young[1]

The abundances of molecules containing more than one rare isotope have been applied broadly to determine formation temperatures of natural materials. These applications of "clumped" isotopes rely on the assumption that isotope-exchange equilibrium is reached, or at least approached, during the formation of those materials. In a closed-system terrarium experiment, we demonstrate that biological oxygen (O_2) cycling drives the clumped-isotope composition of O_2 away from isotopic equilibrium. Our model of the system suggests that unique biological signatures are present in clumped isotopes of O_2—and not formation temperatures. Photosynthetic O_2 is depleted in $^{18}O^{18}O$ and $^{17}O^{18}O$ relative to a stochastic distribution of isotopes, unlike at equilibrium, where heavy-isotope pairs are enriched. Similar signatures may be widespread in nature, offering new tracers of biological and geochemical cycling.

Statistical thermodynamics predicts that heavy isotopes will be bound together in a molecule more often than predicted by chance alone, provided the system is at isotopic equilibrium (*1*, *2*). This preference for heavy-isotope pairing and its variation with temperature forms the basis of clumped-isotope thermometry (*3*–*5*), a class of approaches based on precise measurements of molecules containing more than one rare isotope. When isotope-exchange reactions facilitate the equilibration of heavy-isotope pairs, the resulting isotopic distribution

[1]Department of Earth, Planetary, and Space Sciences, University of California, Los Angeles, CA 90095, USA. [2]Department of Earth Science, Rice University, Houston, TX 77005, USA.
*Corresponding author. E-mail: lyeung@rice.edu (L.Y.Y.); jlash@ucla.edu (J.L.A.) †These authors contributed equally to this work.

has indeed been shown to achieve equilibrium across a wide range of temperatures (*4*, *6*–*8*); however, isotopic equilibrium is the exception rather than the rule in nature. Biogenic substances, for example, are often formed through irreversible enzymatic reactions for which isotope-exchange equilibrium cannot be expected a priori. Yet, many natural materials with kinetically constrained and/or biological origins (e.g., carbonate shells) show only minor departures from equilibrium isotope fractionation (*9*–*11*). Large biological and physical effects on heavy-isotope pairing could complicate the interpretation of emerging clumped-isotope thermometers in methane, O_2, and other candidate systems (*4*, *5*, *12*).

Here, we consider photosynthetic O_2 formation from water at the oxygen-evolving complex of Photosystem II (OEC). In the OEC, O–O bond formation occurs at the end of a five-step light-dependent sequence (Fig. 1). This reaction most likely does not equilibrate O–O isotope pairs given the lack of isotopic equilibration between water and the O_2 produced (*13*–*16*). We argue that the tendency for two heavy oxygen isotopes to be bound together during oxygenic photosynthesis reflects primarily the isotopic preferences of water molecules binding to the OEC. These patterns of heavy-isotope pairing should be apparent in clumped isotopes of O_2. Measurements of the $^{18}O^{18}O$ (mass *36*) and $^{17}O^{18}O$ (mass *35*) isotopologues of O_2, together with bulk isotopic ratios ($^{18}O/^{16}O$ and $^{17}O/^{16}O$), characterize the number of heavy-isotope pairs in a sample relative to the number expected by chance alone (i.e., the stochastic distribution). These deviations are quantified as Δ_{36} and Δ_{35} values: Excesses of $^{18}O^{18}O$ and $^{17}O^{18}O$ relative to the stochastic distribution of isotopes in the sample results in $\Delta_{36} > 0$ and $\Delta_{35} > 0$, respectively. A deficit in $^{18}O^{18}O$ and $^{17}O^{18}O$ results in $\Delta_{36} < 0$ and $\Delta_{35} < 0$.

The Δ_{36} and Δ_{35} signatures of oxygenic photosynthesis can thus be estimated by assigning each water-binding site its own isotopic fractionation factor $\alpha = {}^{18}R_{bound}/{}^{18}R_{water}$, where ^{18}R is the ratio of ^{18}O to ^{16}O atoms in each reservoir. At natural isotopic abundances, the bulk isotopic composition of photosynthetic O_2 is the weighted sum of those contributions—i.e., ${}^{18}R_p \approx \frac{1}{2}[({}^{18}R_{water} \times \alpha_A) + ({}^{18}R_{water} \times \alpha_B)]$, with binding sites A and B each contributing one of two oxygen atoms in each O_2 molecule. The probability of generating ^{18}O–^{18}O bonds is therefore ${}^{36}R_p = ({}^{18}R_{water} \times \alpha_A)({}^{18}R_{water} \times \alpha_B)$. The stochastic distribution of ^{18}O atoms is calculated from the bulk $^{18}O/^{16}O$ ratio as ${}^{36}R_{stochastic} = ({}^{18}R_p)^2$. The expression for $\Delta_{36,p}$ then reduces to (*17*)

$$\Delta_{36,p} = \left[\frac{\alpha_A \alpha_B}{\frac{1}{4}(\alpha_A + \alpha_B)^2} - 1\right] \quad (1)$$

Equation 1 reveals that, in all cases, $\Delta_{36,p} \leq 0$; contrary to the enhanced isotope pairing that would be expected at isotopic equilibrium, there is an apparent aversion to heavy-isotope pairing associated with photosynthetic O_2 production. If the isotopic preferences at each water-binding site are equal ($\alpha_A = \alpha_B$), then $\Delta_{36,p} = 0$. If the binding sites are not equivalent ($\alpha_A \neq \alpha_B$), as isotope-labeling studies indicate (*18*, *19*), then $0 \geq \Delta_{36,p} > -0.9$ per mil (‰) for plausible α-values between 0.97 and 1.03 (*20*, *21*). A similar expression can be derived for $\Delta_{35,p}$ values, which are predicted to be about half those of $\Delta_{36,p}$ (see the supplementary text). These values cannot be interpreted as formation temperatures because all equilibrated samples have $\Delta_n \geq 0$ (*2*). Photosynthesis should therefore impart a distinct non-equilibrium clumped-isotope signature on O_2.

We conducted a closed-system terrarium experiment with six water hyacinths (*Eichhorniae crassipes*) to explore the effects of biological oxygen cycling on five isotopologues of O_2 (*17*). The terrarium was illuminated with fluorescent lights on a 12-hour/12-hour light-dark cycle. Headspace samples were purified and analyzed over a 1-year period for both the bulk and clumped isotopic composition of O_2. We found that biological oxygen cycling altered isotopic ordering in the headspace O_2, yielding apparent steady-state Δ_{36} and Δ_{35} values that are inconsistent with O_2 formation temperatures and more consistent with the predicted photosynthetic endmembers (Fig. 2 and table S3). The Δ_{36} and Δ_{35} values of O_2 were driven down from atmospheric values [2‰ and 1‰, respectively (*4*)] and down past equilibrium values at 25°C (1.5‰ and 0.8‰, respectively), finally approaching an apparent isotopic steady state at the stochastic distribution of isotopes (Δ_{36} = −0.01 ± 0.08‰, and Δ_{35} = 0.0 ± 0.1‰; 1 SEM, n = 4). The plant community shifted to an algae-dominated ecosystem during the first 6 months, altering the isotopic, chemical, and physical properties of the terrarium (fig. S1). However, the clumped-isotope composition of the headspace O_2 evolved steadily toward its apparent steady state, similar to the evolution of the oxygen triple-isotope composition. Steady-state $\Delta'^{17}O$ values were 165 parts per million (ppm), consistent with those reported in similar experiments (*22*, *23*).

Dark incubations of the terrarium, which consumed up to 35% of the headspace O_2, caused Δ_{36} values to increase linearly with time up to ~1‰ (Fig. 2). The Δ_{35} values, in contrast, remained generally constant (means of Δ_{35} = 0.1 ± 0.1‰ and 0.1 ± 0.05‰; 1 SD). Returning to light-dark cycles restored the clumped-isotope composition to its apparent steady-state value after 6 months (Δ_{36} = −0.09 ± 0.06‰, and Δ_{35} = 0.0 ± 0.1‰; 1 SEM, n = 3). To test the veracity of these measurements, headspace O_2 samples drawn from both light and dark incubations were photolytically equilibrated at known temperatures (*4*). The equilibrations yielded Δ_{36} and Δ_{35} values of O_2 consistent with isotope-exchange equilibrium (table S3), suggesting that our observations are unlikely to be analytical artifacts. Atmospheric O_2 leaking into the terrarium would increase $\delta'^{18}O$ far too rapidly relative to Δ_{36} to explain these observations. The observed clumped-isotope variations therefore most likely arise from biological and physical processes inside the terrarium.

We constructed a two-reservoir model of O_2 (i.e., in headspace and water) in the terrarium that accounts for photosynthetic O_2 formation, fractionation of O_2 due to respiration, and air-water gas exchange (*17*). We included kinetic isotope fractionation for gas transfer into and out of solution [${}^{34}\alpha_{GE,kinetic}$ = 0.9972 for $^{18}O/^{16}O$ (*24*)]. The model was run with a range of plausible isotope fractionation factors for respiration [${}^{34}\alpha_R$ = 0.97 – 0.99 (*25*, *26*)] and gas-exchange rates (*24*, *27*) to examine the sensitivity of the terrarium headspace to changes in those quantities. The oxygen triple-isotope composition of the terrarium water was measured and used as the bulk isotopic composition of photosynthetic O_2 (*13*, *15*, *17*). No single set of parameters explained all of the isotopic variations during the entire experiment, likely due to the evolving biological community, so we focus on isotopic variations at steady state and during dark incubations.

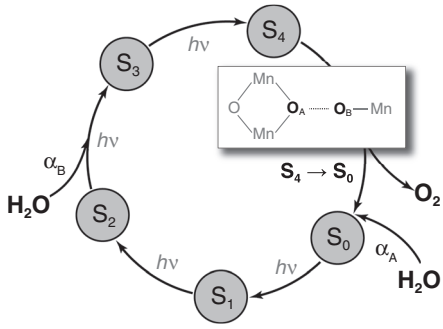

Fig. 1. Conceptual diagram of O_2 formation at the OEC. The five-step Kok cycle for the water-splitting reaction $2H_2O + 4h\nu \rightarrow O_2 + 4H^+ + 4e^-$ is shown without electron flow (*32*). Transitions between intermediate oxidation states of the OEC (S_0 to S_4) occur upon absorption of visible light. The water-binding sequence is based on experimental results (*19*, *33*, *34*), which also indicate that water substrates are exchangeable at least up to state S_3 on chemically distinct binding sites (*18*, *19*). The O–O bond is formed during the S_4-to-S_0 transition, expressing the isotopic fractionations α_A and α_B from water substrate binding.

The increase of headspace Δ_{36} and Δ_{35} values in the dark implies that the apparent steady-state values near zero can only be reached if light-dependent processes drive Δ_{36} and Δ_{35} values below zero. Equation 1 suggests that photosynthesis could be the relevant mechanism, because the O_2 generated is likely to have $\Delta_{36,p}$ and $\Delta_{35,p}$ values less than zero. To estimate the composition of this source, we note that kinetic and equilibrium isotope effects for relevant photosynthetic fractionations are probably in the range $0.96 > {}^{18}\alpha > 1.04$ (*20*, *21*), which we broaden to a more conservative plausible range of $0.9 > {}^{18}\alpha > 1.1$. This range of isotope effects gives lower limits on $\Delta_{36,p}$ and $\Delta_{35,p}$ of −10‰ and −5‰, respectively.

If the Δ_{36} increase during dark incubations were solely caused by fractionation in respiration, then large isotope effects in water-enzyme binding would be required: $\Delta_{36,p} < -10$‰ is needed to achieve steady-state values of Δ_{36} near zero (*17*). In addition, the associated $\Delta_{35,p} < -5$‰

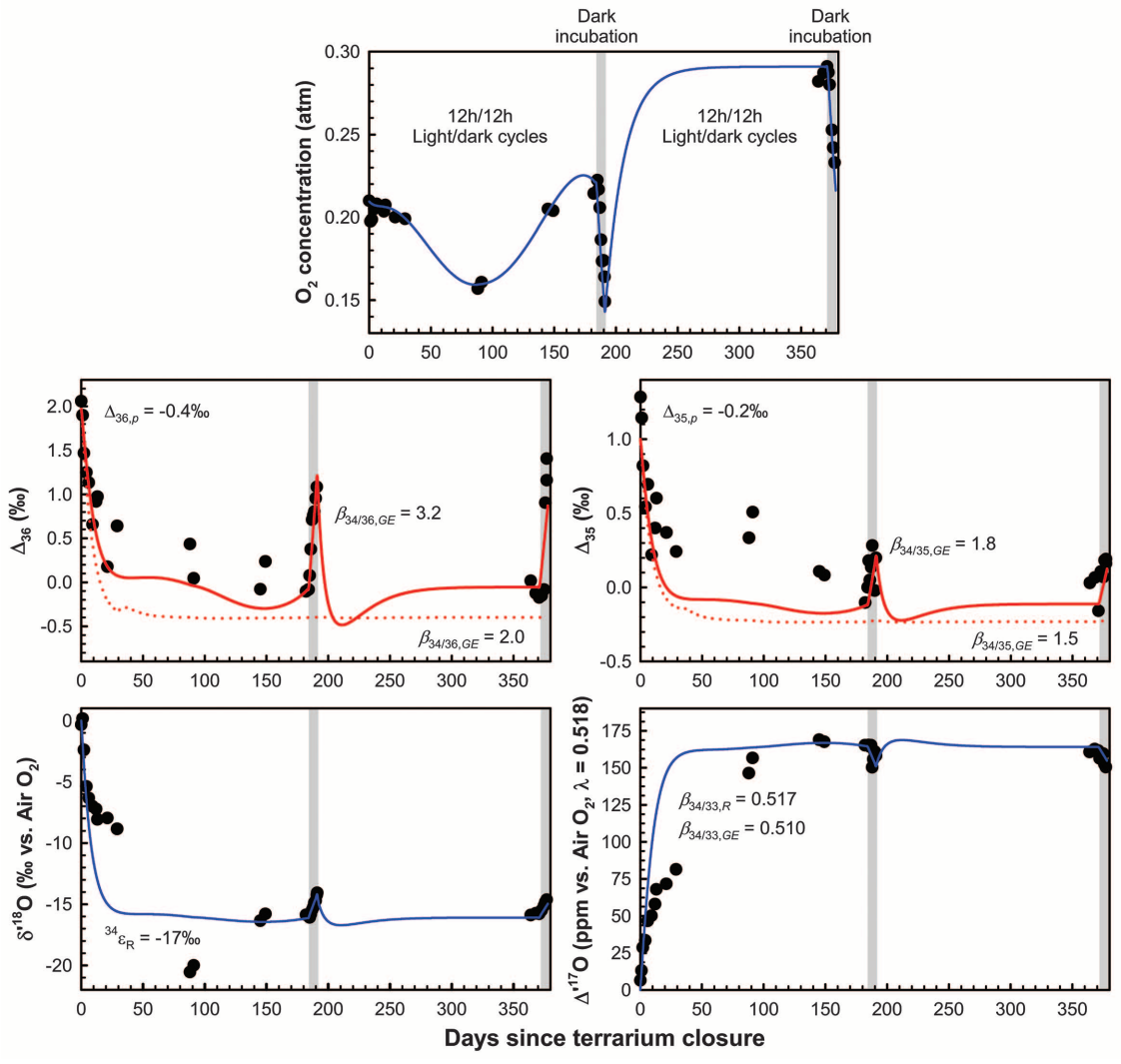

Fig. 2. Evolution of concentration and O_2 isotopologue composition in the terrarium. Observations (data points) are compared with model results (curves). Uncertainties are not shown for clarity, but long-term analytical uncertainties in O_2 concentration, $\delta'^{18}O$, $\Delta'^{17}O$, Δ_{36}, and Δ_{35} are 1%, 0.04‰, 5 ppm, 0.17‰, and 0.3‰, respectively. A single isotopologue discrimination factor ($^{34}\varepsilon_R$ = −17‰) is used here to illustrate steady-state behavior in $\delta'^{18}O$ and $\Delta'^{17}O$; a more detailed model run yields better agreement for $\delta'^{18}O$ and $\Delta'^{17}O$ but similar results for Δ_{36} and Δ_{35}. Mass-dependent exponents used in the model, $\beta_{34/n}$, are labeled, with subscripts *R* and *GE* denoting values for respiration and gas exchange, respectively. For $\beta_{34/35,GE}$ and $\beta_{34/36,GE}$, two model runs are shown to illustrate their effects on the Δ_{36} and Δ_{35} time traces (*17*).

endmember composition causes poor agreement between measured and modeled Δ_{35} values (fig. S4C). Furthermore, an increase in respiration rates would drive Δ_{36} and Δ_{35} values higher, whereas a decrease in respiration rates would drive the O_2 toward its $\Delta_{36,p}$ and $\Delta_{35,p}$ photosynthetic values (*17*). Therefore, when the O_2 cycle was out of balance in the first 6 months, Δ_{36} would have fluctuated inversely with O_2 concentration (fig. S4, B and C). Instead, both Δ_{36} and Δ_{35} decreased nearly monotonically.

Isotopologue fractionation during nonequilibrium O_2 gas exchange could explain the increases of headspace Δ_{36} and Δ_{35} values during dark incubations. The fractionation in headspace $^{16}O^{18}O/^{16}O_2$ is closer to that for gas exchange than that for respiration ($^{34}\alpha_{observed}$ = 0.995 versus $^{34}\alpha_{GE,kinetic}$ = 0.9972 versus $^{34}\alpha_R$ ~ 0.98), suggesting that the Δ_{36} and Δ_{35} increases are similarly dominated by gas exchange. Modeling the mass dependence of gas exchange using the dark incubation data yields $\Delta_{36,p}$ and $\Delta_{35,p}$ values within a plausible range (i.e., $\Delta_{36,p}$ = −0.4‰, $\Delta_{35,p}$ = −0.2‰) (Fig. 2). The evolution of Δ_{36} and Δ_{35} is also more robust to imbalances in the O_2 cycle (*17*). Other oxygen-consumption mechanisms, such as sulfide oxidation, could impart additional isotopologue signatures (*28*), so attributing isotopologue discrimination in the dark to a single process is necessarily a simplification. Indeed, the implied mass dependence of O_2 consumption in the dark terrarium is unusual, and it merits further investigation (*17*). A detailed understanding of isotopologue fractionation factors will require more controlled experiments of isolated biological and physical processes. Yet, the specific isotopologue discrimination during dark incubations does not affect the conclusion that photosynthesis generates O_2 with an "anticlumped" isotopologue distribution (i.e., $\Delta_{36} \leq 0$ and $\Delta_{35} \leq 0$). This biological signature in O_2 may be readily observed in the surface ocean, where it could be used to constrain gross primary productivity by exploiting the contrast between biological and atmospheric O_2 clumped-isotope signatures (*29*). Isotopic ordering in atmospheric O_2 is relatively unaffected by biological O_2 cycling because photochemical equilibration of O_2 exceeds rates of biological cycling by at least a factor of 100 (*4*, *30*). Using a biological endmember composition of Δ_{36} = 0, we calculate that biological effects on the tropospheric Δ_{36} budget are therefore most likely on the order of 0.01‰.

Our observations indicate that variations in the isotopologue abundance of even simple molecules like O_2 capture the chemistry of complex natural systems. Broader application of these techniques could yield insights into the mechanisms of biomolecule synthesis, e.g., methanogenesis, nitrogen reduction during denitrification, and molecular hydrogen release during nitrogen fixation (*31*). Moreover, because clumped-isotope signatures can depend only on isotope fractionation factors and not on the isotopic composition of substrates, a new class of reservoir-insensitive approaches for tracing biogeochemical cycling could emerge from these molecular-scale insights.

REFERENCES AND NOTES

1. P. Richet, Y. Bottinga, M. Javoy, *Annu. Rev. Earth Planet. Sci.* **5**, 65–110 (1977).
2. Z. Wang, E. A. Schauble, J. M. Eiler, *Geochim. Cosmochim. Acta* **68**, 4779–4797 (2004).
3. P. Ghosh *et al.*, *Geochim. Cosmochim. Acta* **70**, 1439–1456 (2006).

4. L. Y. Yeung, J. L. Ash, E. D. Young, *J. Geophys. Res.* **119**, 10 (2014).
5. D. A. Stolper *et al.*, *Science* **344**, 1500–1503 (2014).
6. H. P. Affek, *Am. J. Sci.* **313**, 309–325 (2013).
7. B. H. Passey, G. A. Henkes, *Earth Planet. Sci. Lett.* **351-352**, 223–236 (2012).
8. D. A. Stolper *et al.*, *Geochim. Cosmochim. Acta* **126**, 169–191 (2014).
9. W. Guo, J. L. Mosenfelder, W. A. Goddard III, J. M. Eiler, *Geochim. Cosmochim. Acta* **73**, 7203–7225 (2009).
10. J. Tang, M. Dietzel, A. Fernandez, A. K. Tripati, B. E. Rosenheim, *Geochim. Cosmochim. Acta* **134**, 120–136 (2014).
11. H. P. Affek, S. Zaarur, *Geochim. Cosmochim. Acta* **143**, 319–330 (2014).
12. S. Ono *et al.*, *Anal. Chem.* **86**, 6487–6494 (2014).
13. R. D. Guy, M. L. Fogel, J. A. Berry, *Plant Physiol.* **101**, 37–47 (1993).
14. C. L. R. Stevens, D. Schultz, C. Van Baalen, P. L. Parker, *Plant Physiol.* **56**, 126–129 (1975).
15. Y. Helman, E. Barkan, D. Eisenstadt, B. Luz, A. Kaplan, *Plant Physiol.* **138**, 2292–2298 (2005).
16. H. C. Urey, L. J. Grieff, *J. Am. Chem. Soc.* **57**, 321–327 (1935).
17. Materials and methods are available as supplementary materials on *Science* Online.
18. W. Hillier, T. Wydrzynski, *Coord. Chem. Rev.* **252**, 306–317 (2008).
19. L. Rapatskiy *et al.*, *J. Am. Chem. Soc.* **134**, 16619–16634 (2012).
20. A. M. Angeles-Boza *et al.*, *Chem. Sci.* **5**, 1141 (2014).
21. A. M. Angeles-Boza, J. P. Roth, *Inorg. Chem.* **51**, 4722–4729 (2012).
22. B. Luz, E. Barkan, M. L. Bender, M. H. Thiemens, K. A. Boering, *Nature* **400**, 547–550 (1999).
23. A. Angert, S. Rachmilevitch, E. Barkan, B. Luz, *Global Biogeochem. Cycles* **17**, 1030 (2003).
24. M. Knox, P. D. Quay, D. Wilbur, *J. Geophys. Res.* **97** (C12), 20335–20343 (1992).
25. B. Luz, E. Barkan, *Geochim. Cosmochim. Acta* **69**, 1099–1110 (2005).
26. M. H. Cheah *et al.*, *Anal. Chem.* **86**, 5171–5178 (2014).
27. K. E. Tempest, S. Emerson, *Mar. Chem.* **153**, 39–47 (2013).
28. R. S. Thurston, K. W. Mandernack, W. C. Shanks III, *Chem. Geol.* **269**, 252–261 (2010).
29. L. W. Juranek, P. D. Quay, *Annu. Rev. Mar. Sci.* **5**, 503–524 (2013).
30. L. Y. Yeung, E. D. Young, E. A. Schauble, *J. Geophys. Res.* **117**, D18306 (2012).
31. B. M. Hoffman, D. Lukoyanov, D. R. Dean, L. C. Seefeldt, *Acc. Chem. Res.* **46**, 587–595 (2013).
32. B. Kok, B. Forbush, M. McGloin, *Photochem. Photobiol.* **11**, 457–475 (1970).
33. T. Noguchi, *Phil. Trans. R. Soc. B.* **363**, 1189–1195 (2008).
34. N. Cox *et al.*, *Science* **345**, 804–808 (2014).

ACKNOWLEDGMENTS

We thank H. Hu and N. Levin for performing oxygen triple-isotope analyses of the terrarium water at Johns Hopkins University, and E. Schauble for helpful discussions during the course of this work. This research was supported in part by the National Science Foundation (EAR-1049655 and DGE-1144087), the National Aeronautics and Space Administration Cosmochemistry program, and the Deep Carbon Observatory. The data and model parameters used in this study are available in the supplementary materials (tables S1 to S3).

SUPPLEMENTARY MATERIALS

www.sciencemag.org/content/348/6233/431/suppl/DC1
Materials and Methods
Supplementary Text
Figs. S1 to S5
Tables S1 to S3
References (*35*–*50*)

7 January 2015; accepted 13 March 2015
10.1126/science.aaa6284

RESEARCH FUNDING

Big names or big ideas: Do peer-review panels select the best science proposals?

Danielle Li[1]*† and Leila Agha[2,3]*†

This paper examines the success of peer-review panels in predicting the future quality of proposed research. We construct new data to track publication, citation, and patenting outcomes associated with more than 130,000 research project (R01) grants funded by the U.S. National Institutes of Health from 1980 to 2008. We find that better peer-review scores are consistently associated with better research outcomes and that this relationship persists even when we include detailed controls for an investigator's publication history, grant history, institutional affiliations, career stage, and degree types. A one–standard deviation worse peer-review score among awarded grants is associated with 15% fewer citations, 7% fewer publications, 19% fewer high-impact publications, and 14% fewer follow-on patents.

In 2014, the combined budgets of the U.S. National Institutes of Health (NIH), the U.S. National Science Foundation, and the European Research Council totaled almost $40 billion. The majority of these funds were allocated to external researchers whose applications were vetted by committees of expert reviewers. But as funding has become more competitive and application award probabilities have fallen, some observers have posited that "the system now favors those who can guarantee results rather than those with potentially path-breaking ideas that, by definition, cannot promise success" (*1*). Despite its importance for guiding research investments, there have been few attempts to assess the efficacy of peer review.

Peer-review committees are unique in their ability to assess research proposals based on deep expertise but may be undermined by biases, insufficient effort, dysfunctional committee dynamics, or limited subject knowledge (*2*, *3*). Disagreement about what constitutes important research may introduce randomness into the process (*4*). Existing research in this area has focused on understanding whether there is a correlation between good peer-review scores and successful research outcomes and yields mixed results (*5*–*7*). Yet raw correlations do not reveal whether reviewers are generating insight about the scientific merit of proposals. For example, if applicants from elite institutions generally produce more highly cited research, then a system that rewarded institutional rankings without even reading applications may appear effective at identifying promising research.

In this paper, we investigate whether peer review generates new insights about the scientific quality of grant applications. We call this ability peer review's "value-added." The value-added of NIH peer review is conceptually distinct from the value of NIH funding itself. For example, even if reviewers did a poor job of identifying the best applications, receiving a grant may still improve a researcher's productivity by allowing her to maintain a laboratory and support students. Whereas previous work has studied the impact of receiving NIH funds on the productivity of awardees (*8*, *9*), our paper asks whether NIH selects the most promising projects to support. Because NIH cannot possibly fund every application it receives, the ability to distinguish potential among applications is important for its success.

We say that peer review has high value-added if differences in grants' scores are predictive of differences in their subsequent research output, after controlling for previous accomplishments of the applicants. This may be the case if reviewers generate additional insights about an application's potential, but peer review may also have zero or even negative value-added if reviewers are biased, mistaken, or focused on different goals (*10*).

Because research outcomes are often skewed, with many low-quality or incremental contributions and relatively few ground-breaking discoveries (*2*, *11*), we assess the value-added of peer review for identifying research that is highly influential or shows commercial promise. We also test the effectiveness of peer review in screening out applications that result in unsuccessful research (see the supplementary materials for full details on data and methods).

NIH is the world's largest funder of biomedical research (*12*). With an annual budget of approximately $30 billion, it supports more than 300,000 research personnel at more than 2500 institutions (*12*, *13*). A funding application is assigned by topic to one of approximately 200 peer-review committees (known as study sections).

Our main explanatory variable is the "percentile score," ranging from 0 to 100, which reflects an application's ranking among all other applications reviewed by a study section in a given fiscal year; lower scores correspond to higher-quality applications. In general, applications are funded in order of their percentile score until the budget of their assigned NIH institute is exhausted. The average score in our sample is 14.2, with a standard deviation (SD) of 10.2; only about 1% of funded grants in our sample had a score worse than 50. Funding has become more competitive in recent years; only 14% of applications were funded in 2013.

[1]Harvard University, Cambridge, MA 02138, USA. [2]Boston University, Boston, MA 02215, USA. [3]National Bureau of Economic Research, Cambridge, MA 02138, USA.
***Corresponding author. E-mail: dli@hbs.edu (D.L.); lagha@bu.edu (L.A.)** †Both authors contributed equally to this work.

Biological signatures in clumped isotopes of O_2

Laurence Y. Yeung *et al.*

Science **348**, 431 (2015);
DOI: 10.1126/science.aaa6284

Science (print ISSN 0036-8075; online ISSN 1095-9203) is published weekly, except the last week in December, by the American Association for the Advancement of Science, 1200 New York Avenue NW, Washington, DC 20005.